American Mineralogist, Volume 71, pages 264–276, 1986

Hydrogen and the melting of silicates[1]

ROBERT W. LUTH,[2] A. L. BOETTCHER
Institute of Geophysics and Planetary Physics and Department of Earth and Space Sciences
University of California, Los Angeles, Los Angeles, California 90024

ABSTRACT

The solidi of albite, diopside, and quartz in the presence of H_2O-H_2 vapors have been determined from 5 to 30 kbar for vapors buffered by the assemblages iron-wüstite-H_2O (IW), hematite-magnetite-H_2O (HM), and pure H_2O. As the activity of H_2 in the vapor increases, the solidi in these systems increase systematically in temperature. The difference between the solidus of silicate + H_2O and that of silicate + H_2O + H_2 (HM) in all three systems is larger than could result from simple dilution of the vapor by H_2, implying that H_2 dissolves in the silicate liquid and inhibits the solution of H_2O. Comparison of these results with data for the analogous H_2O + CO_2 systems suggests that H_2 is more soluble than CO_2 in these liquids under similar conditions of pressure and temperature. Variations in f_{H_2} and f_{O_2} in experimental apparatus in different laboratories can explain many apparent inconsistencies in experimental results. These systems also serve as models for melting and metasomatism under conditions of f_{O_2} and f_{H_2} consistent with values postulated for the Earth.

INTRODUCTION

The influence of volatile components, particularly H_2O, on phase relations in silicate systems has been intensively investigated for a number of years. The emphasis on the effect of H_2O stems from petrologic and experimental grounds. In magmas, H_2O is the dominant volatile, as revealed by analyses of volcanic gases and glasses. In the laboratory, H_2O lowers melting temperatures as much as hundreds of degrees, and it is an efficacious flux, greatly enhancing reaction rates and the attainment of equilibrium.

Nevertheless, H_2O-saturated conditions appear only under exceptional conditions in magmas, prompting petrologists to study silicate-H_2O systems at H_2O-undersaturated conditions. To achieve H_2O-undersaturated conditions in the laboratory, the hydrous vapor is diluted with another component, commonly CO_2, which is the second-most-abundant volatile component in volcanic gases (Gerlach and Nordlie, 1975; Gerlach, 1982). However, Hill and Boettcher (1970) determined that CO_2 dissolves in some silicate liquids at pressures above ~15 kbar based on the shapes and relative positions of the basalt-H_2O and basalt-H_2O-CO_2 solidi. Subsequently, there have been numerous studies of H_2O + CO_2-bearing systems to assess the effect of these volatiles on melting in the mantle (Mysen and Boettcher, 1975; Brey and Green, 1977; Eggler, 1978; Wyllie, 1979), to determine thermodynamic properties of H_2O-CO_2 fluids at high pressures (Eggler and Kadik, 1979; Bohlen et al., 1982, 1983), and to determine the mechanisms of solution of the volatiles and their effect on the structural and rheological properties of silicate liquids (Burnham, 1979; Mysen and Virgo, 1980; Stolper, 1982; Boettcher, 1984).

Our work focuses on a mixed-volatile system that has not been considered in any detail to date: the H_2O-H_2 system. This system is important in both geologic and experimental situations, because of the dissociation reaction

$$H_2O[v] = H_2[v] + \tfrac{1}{2}O_2[v].$$

In the presence of an assemblage that buffers the oxygen fugacity (f_{O_2}) at a fixed value, the ratio of the fugacity of H_2O (f_{H_2O}) to the fugacity of H_2 (f_{H_2}) is fixed at a given pressure and temperature. With the additional constraint that the bulk composition of the vapor is in the O-H system, the composition of the vapor is invariant. Silicate components are negligible, typically composing <1 mol% of the vapor. In natural assemblages, there may be an oxidation-reduction reaction such as the following:

$$2Fe_2O_3[1] = 4FeO[1] + O_2,$$

where Fe_2O_3 and FeO represent ferric and ferrous components in the silicate liquid (Kennedy, 1948; Sack et al., 1980). Other assemblages, which lack a silicate liquid but contain Fe, may also buffer the f_{O_2} (Greenwood, 1975).

In the laboratory, the buffering reaction may be the oxidation of the walls of the pressure vessel by the gas pressure medium, or degassing and dehydration of the furnace assembly in solid-media high-pressure apparatus. Alternatively, f_{O_2} may be controlled by gas mixtures of CO_2 + H_2 or CO_2 + CO, or by oxygen buffers such as hematite + magnetite + H_2O (HM) or iron + wüstite + H_2O (IW). Even a vapor of nominally pure H_2O contains

[1] Institute of Geophysics and Planetary Physics Contribution No. 2628.

[2] Present address: Geophysical Laboratory, 2801 Upton Street, N.W., Washington, D.C. 20008.

0003–004X/86/0304–0264$02.00

a finite amount of H_2 and O_2 because of the dissociation reaction. In this case, the composition of this vapor is fixed at a given pressure and temperature by the dissociation reaction of H_2O, the restriction to a binary O-H vapor, and the restriction that the bulk composition remains H_2O. Oxygen buffers, from the most oxidizing one that is commonly used (HM) to the most reducing one (IW), all have lower f_{O_2} and higher f_{H_2} than does pure H_2O.

Previous work on the effect of H_2 on the phase relations of silicates is sparse. Nakamura (1974) studied the system SiO_2-H_2O-H_2 at 15 kbar and f_{H_2} buffered by the talc furnace assembly (~HM) and by the IW buffer. When buffered by the furnace assembly at low f_{H_2}, the system was supercritical, with a single fluid phase rather than discrete liquids and vapors, consistent with previous work on SiO_2-H_2O that indicated a critical end-point at ~10 kbar (Kennedy et al., 1962). In contrast, when the system was buffered by IW at higher f_{H_2}, the liquid and vapor were distinguishable, indicating that H_2 increased the critical point to >15 kbar.

Faile et al. (1967) and Faile and Roy (1970, 1971) studied the solubility of H_2 in SiO_2 glasses quenched from 800°C and P_{H_2} <3 kbar. Even at these low temperatures and pressures and without H_2O, they produced glasses with up to ~8 mol% H_2. They did not study the effect of H_2 on the phase relations of SiO_2.

To examine the effect of high f_{H_2} on silicate phase relations, we have determined vapor-saturated solidi in the systems SiO_2-H_2O-H_2, $NaAlSi_3O_8$-H_2O-H_2, and $CaMgSi_2O_6$-H_2O-H_2 at pressures between 5 and 30 kbar. We controlled f_{H_2} by using a wide range of buffers. Because the composition of the vapor in equilibrium with the buffer assemblages changes with pressure and temperature, the mole fraction of H_2O in the vapor ($X^v_{H_2O}$) changes along the vapor-saturated solidi, which complicates comparisons with the analogous systems containing H_2O + CO_2, with fixed $X^v_{H_2O}$ along a given solidus. However, we can use this sytem in solid-media high-pressure apparatus and thereby study these reactions at higher pressures than attainable in a gas-pressurized apparatus.

Experimental techniques

Starting materials

The diopside was synthesized from MgO and CaO (both Puratronic grade, from Johnson Matthey Chemicals) and natural quartz. The CaO was fired at 1000°C for 24 h prior to weighing. The MgO was fired at 1000°C for 24 h, then 1500°C for 4 h, followed by 16 h at 1000°C prior to weighing. The quartz is that used in the study of SiO_2-H_2O-CO_2 by Boettcher (1984); it was ground, boiled in HNO_3, rinsed thoroughly in distilled H_2O, and fired at 1000°C for 24 h before weighing. The oxides were weighed in stoichiometric proportions, mixed thoroughly, and fused at 1450°C for 8 h, quenched, reground, and remelted several times until a homogeneous glass was obtained. This glass was crystallized at 1-atm pressure, 1300°C for 12 h, then recrystallized hydrothermally at 5 kbar, 1100°C for 24 h. This resulted in well-crystallized, moderately fine grained (10–20 μm) diopside.

The albite is a natural albite from the Franciscan Formation of California that contains 0.03 wt% CaO, 0.04 wt% K_2O, 0.01 wt% Fe_2O_3, and 0.003 wt% MgO. For most experiments, the albite was in the low structural state. This material is ideal for melting reactions in $NaAlSi_3O_8$-H_2O-H_2, because above ~3 kbar, low albite is the stable polymorph at temperatures near the albite + H_2O solidus (Goldsmith and Jenkins, 1984). For some experiments, the albite was converted to the high structural state by recrystallization at 20 kbar, 1200°C for 24 h. In contrast to the rapid disordering of low albite, the ordering of high albite takes months at the conditions of interest, and therefore high albite persists metastably for the duration of our experiments.

Approximately 5 mg of the appropriate starting material, together with deionized, distilled H_2O, were sealed into 1.6-mm diameter Pt capsules. Masses were measured to the nearest microgram on a Mettler M3 microbalance and were reproducible to ± 3 μg. The inner capsule containing silicate + H_2O was sealed inside a 3.5-mm diameter Pt capsule together with the buffer assemblage, either iron-wüstite-H_2O (IW), wüstite-magnetite-H_2O (WM), nickel–nickel oxide–H_2O (NNO), or hematite-magnetite-H_2O (HM). The buffer assemblage fixes the f_{H_2} in the buffer capsule; diffusion of H_2 through the wall of the inner capsule buffers the f_{H_2} inside the sample capsule, in turn fixing the f_{O_2} and f_{H_2O} in the sample capsule.

Most of the pure-H_2O experiments were run without an outer capsule. Previous experiments, using samples of different buffer assemblages, established that the f_{H_2} of the furnace assembly at conditions of interest to this study was lower than that of the HM buffer, as expected because of the lack of hydrous parts in the furnace assembly (Boettcher et al., 1981). Therefore, influx of H_2 into the capsule was negligible, and thus these experiments were in the silicate + H_2O subsystem. To insure that there were no thermal effects because of no outer capsule, we loaded quartz into an outer capsule, together with the sample capsule, mimicking the thermal situation of the other experiments where the double-capsule technique was used. The results of this experiment were consistent with those using a single capsule.

Apparatus and run procedure

The experiments were run in piston-cylinder apparatus, using 2.54-cm diameter furnace assemblies composed of NaCl, pyrex, graphite, BN, and MgO (Boettcher et al., 1981). Temperatures were monitored using Pt-$Pt_{90}Rh_{10}$ thermocouples encased in mullite ceramic, with the tip of the thermocouple in contact with the capsule. We used the hot piston-in technique by bringing the pressure to about 5% below the final value, then increasing temperature and finally pressure to the desired values. The experiments were controlled with a precision of ± 2°C and ± 0.05 kbar. At the end of the run, the experiment was quenched by shutting off the power, resulting in a temperature drop of 500°C or more within 20 s, and to room temperature in less than 3 min.

Following the run, the buffer capsule was weighed, punctured, heated, and then reweighed to confirm that H_2O was present. Optical microscopy or X-ray diffraction confirmed the presence of the required solid phases of the buffer. The sample capsule was cleaned, weighed, punctured, heated at 112°C, and then reweighed. A weight loss at this stage confirmed that H_2O remained in the capsule throughout the experiment. In typical hypersolidus experiments, the weight loss was 75–90% of the amount of H_2O originally loaded in the capsule, indicating that some H_2O remained in the quenched liquid. However, the weight losses for capsules from hyperliquidus experiments indicate that >50% of the volatiles exsolved from the liquid during the quenching of the experiment. After the sample capsule was opened, the products were examined in immersion oils using a petrographic microscope.

Run products

The nature of the run products differed somewhat from system to system. In the $NaAlSi_3O_8$-H_2O-H_2 and SiO_2-H_2O-H_2 systems, quenched liquids were always bubble-rich glasses that had nearly completely degassed during the quench. In the $CaMgSi_2O_6$-H_2O-H_2 systems, liquids quenched to crystals, either large, single crystals with many vapor bubbles, glassy inclusions, and undulatory or patchy extinction, or radial sheaves of crystals with interstitial glass. In either case, the quenched liquid was clearly distinguishable from the well-crystalized, usually smaller crystals of primary diopside.

In all three systems, vapor quenched to "fish-roe"—small, isotropic, glass spheres of lower refractive index than quenched liquid. In the SiO_2-H_2O-H_2 system, vapor also quenched to large, thin plates of bubble-free glass, which often appeared to have formed from coalesced fish-roe spheres. These plates of vapor could be distinguished from quenched liquid by their lack of bubbles and lower index of refraction ($n < 1.50$). At pressures above the critical points in SiO_2-H_2O-H_2, liquid and vapor were indistinguishable; there was a single fluid phase that became increasingly abundant at the expense of the crystalline quartz as the temperature increased. In the $CaMgSi_2O_6$-H_2O-H_2 system, at pressures above ~25 kbar, vapor commonly quenched as large, thin plates or acicular pieces of isotropic, or nearly isotropic, material of low refractive index ($n < 1.50$).

To ensure equilibrium, runs were reversed at several pressures in all three systems. These were done by first subjecting a sample to conditions of pressure, temperature, and run duration, known from our other experiments to be sufficient to melt, or partially melt, the charge. The temperature was then lowered to below the solidus determined by previous runs. Run products in a successful reversal contained no quenched liquid. Data for intracrystalline diffusion of hydrogen through Pt (Ebisuzaki et al., 1968) indicate that equilibrium with respect to f_{H_2} would be established between the buffer and sample capsules in <5 s even at the lowest temperatures studied.

Calculation of vapor composition

The composition of the H_2O-H_2 vapor was calculated using the expressions for f_{O_2} for the various buffers from Huebner (1971), the free energy of dissociation of H_2O from Robie et al. (1979), and the modified Redlich-Kwong (MRK) equation of state of Holloway (1977). When buffered by an O_2 buffer, the $X^v_{O_2}$ was always orders of magnitude less than the $X^v_{H_2}$, and the vapors were considered to be binary H_2O-H_2 mixtures. Because of the many factors of varying precision used in the calculation, there are large uncertainties in the $X^v_{H_2}$. The f_{O_2} of the buffer was calculated from experimental data at atmospheric pressure and the molar volumes of the solid phases; these extrapolations have been experimentally constrained only at 2 kbar (Chou, 1978). For example, changing log (f_{O_2}) by 1 changes $X^v_{H_2}$ for a HM-buffered vapor by a factor of 3. Uncertainties in the free energy of dissociation for H_2O lead to uncertainties in the f_{H_2}/f_{H_2O} ratio and thereby in the $X^v_{H_2O}$. An error in the free energy of dissociation of H_2O of 10% may change $X^v_{H_2}$ for a HM-buffered vapor by a factor of 15. The MRK equation of state, used to convert f_{H_2} to $X^v_{H_2}$, has potentially large uncertainties for two reasons. First, there are no fugacity data for pure H_2 or H_2-H_2O mixtures at pressures higher than 3 kbar (Shaw, 1963; Shaw and Wones, 1964; Presnall, 1969) or for H_2O above 10 kbar (Burnham et al., 1969) against which to calibrate the MRK equation. Second, the MRK equation uses a simple mixing rule that may not be realistic for H_2O-H_2 vapors at the conditions of our experiments. In this regard, it should be noted that de Santis et al. (1974), the authors who published the modification of the Redlich-Kwong equation of state used by Holloway (1977), specifically stated that because of the simplifications used in the formulation of this equation of state, it would not provide highly accurate results, and furthermore, they recommended that the equation be used in the region 25–700°C and at pressures up to 1500 bars.

Results

Experimental results are presented in Tables 1 through 3 and Figures 1 through 4. There are two features that the systems studied share. First, increasing f_{H_2} at a given pressure systematically increases the temperature of the vapor-saturated solidus, with a large difference between the pure-H_2O and HM-buffered solidi, disproportionate to the increase in the calculated $X^v_{H_2}$. Second, the amount of quenched vapor observed in the run products decreases as $X^v_{H_2}$ increases, indicating that the solubility of silicates in the vapor decreases with decreasing $X^v_{H_2O}$, similar to results for systems containing H_2O + CO_2 (Shettel, 1973; Eggler, 1975; Boettcher, 1984). For simplicity, individual features of the three systems will be presented in turn.

$CaMgSi_2O_6$-H_2O-H_2

There is a large (~80°) temperature difference between the pure-H_2O solidus and that buffered by HM at ~10 kbar, but the difference decreases with increasing pressure (Fig. 1). For the IW-buffered solidus, there is a pronounced temperature minimum between 15 and 24 kbar. Below 15 kbar, the IW-buffered solidus is ~100°C higher than the solidus for pure H_2O, whereas above 15 kbar, the difference between the two solidi increases to ~130°C at 27.5 kbar.

$NaAlSi_3O_8$-H_2O-H_2

In contrast to the results for the $CaMgSi_2O_6$-H_2O-H_2 system, there are no abrupt changes in slope for the solidus of $NaAlSi_3O_8$-H_2O-H_2 (IW), although we examined this system only to ~17 kbar because of the reaction of albite to jadeite + quartz (Fig. 2). The difference in temperature between the pure-H_2O and the IW-buffered solidi remains relatively constant at ~50°C.

Following the study of Goldsmith and Jenkins (1984) on the effect of the structural state of albite on vapor-present melting, we determined the metastable vapor-saturated solidus of high albite + H_2O (Fig. 3), which is at lower temperatures than the stable solidus of low albite + H_2O. This temperature difference agrees with the data of Goldsmith and Jenkins (1984), and it is in accord with the requirement that the metastable polymorph melts at a lower temperature than does the stable polymorph. Comparison of the X-ray diffractograms of the albite before and after the experiments showed no ordering during the experiments.

SiO_2-H_2O-H_2

As in the other systems, increasing f_{H_2} at a given pressure increases the temperature of the vapor-saturated solidus of quartz + vapor, and again, there is a measurable dif-

Table 1. Experimental results for $CaMgSi_2O_6$-H_2O-H_2

Run #	P kbar	T °C	H_2O loaded wt%	$X^V_{H_2}$	Duration h	Results
Pure H_2O						
1012	7.5	1170	17.1	3.0×10^{-7}	3	Di+V
1016	7.5	1180	13.8	3.4×10^{-7}	3	Di+V
1008	7.5	1190	18.6	3.8×10^{-7}	3	Di+L+V
1021	7.5	1190	15.0	3.8×10^{-7}	8	Di+L+V
994	7.5	1200	15.8	4.3×10^{-7}	3	Di+L+V
1007	7.5	1210	19.3	4.8×10^{-7}	3	Di+L+V
1186R	7.5	1190	20.5	3.8×10^{-7}	3	(see #1008)
⟶	7.5	1175		3.2×10^{-7}	3	Di+V
1005	10	1170	15.5	5.6×10^{-8}	3	Di+V
1009	10	1170	31.6	5.6×10^{-8}	3	Di+V
992	10	1180	17.5	6.4×10^{-8}	3	Di+V
990	10	1190	19.3	7.4×10^{-8}	3	Di+L+V
987	10	1190	42.1	7.4×10^{-8}	3	Di+L+V
985	10	1200	18.3	8.5×10^{-8}	9	Di+L+V
982	10	1210	14.7	9.9×10^{-8}	3	Di+L+V
967	10	1220	16.7	1.1×10^{-7}	3	Di+L+V
966*	10	1230	18.3	1.3×10^{-7}	3	Di+L+V
915	10	1240	17.8	1.5×10^{-7}	2	Di+L+V
1189R	10	1190	21.7	7.4×10^{-8}	3	(see # 987)
⟶	10	1175		6.0×10^{-8}	3	Di+V
1024	20	1170	17.5	2.5×10^{-17}	3	Di+V
1023	20	1180	14.7	5.0×10^{-17}	3	Di+L+V
1003	20	1190	20.4	9.7×10^{-17}	3	Di+L+V
1023	20	1200	15.6	1.8×10^{-16}	3	Di+L+V
1004	20	1210	17.8	3.6×10^{-16}	3	Di+L+V
1018	20	1220	17.8	7.0×10^{-16}	3	Di+L+V
1015	27.5	1170	19.3	$< 10^{-20}$	3	Di+V
1213	27.5	1180	18.2	$< 10^{-20}$	0.5	Di+V
1014	27.5	1190	18.9	$< 10^{-20}$	3	Di+L+V
HM Buffer						
695	7.5	1200	26.6	1.0×10^{-5}	15	Di+V
696	7.5	1220	26.8	1.1×10^{-5}	15	Di+V
691	7.5	1240	23.0	1.1×10^{-5}	15	Di+V
702	7.5	1250	24.4	1.1×10^{-5}	15	Di+V
682	7.5	1260	23.5	1.1×10^{-5}	2	Di+V
718	7.5	1260	30.1	1.1×10^{-5}	18	Di+V
676	7.5	1270	26.8	1.1×10^{-5}	2	Di+L+V
677	7.5	1280	19.3	1.2×10^{-5}	2	Di+L+V
1187R	7.5	1270	19.9	1.1×10^{-5}	3	(see # 676)
⟶	7.5	1255		1.1×10^{-5}	3	Di+V
644	10	1220	23.6	7.5×10^{-6}	2	Di+V
725	10	1230	22.2	7.6×10^{-6}	23	Di+V
735	10	1240	23.2	7.8×10^{-6}	18	Di+V
920	10	1250	14.3	7.9×10^{-6}	2	Di+V
642	10	1250	23.8	7.9×10^{-6}	2	Di+V
921	10	1260	17.1	8.0×10^{-6}	2	Di+V
639	10	1260	19.7	8.0×10^{-6}	2	Di+(L)+V
922	10	1270	18.1	8.1×10^{-6}	2	Di+L+V
726	10	1280	17.7	8.2×10^{-6}	18	L+V
736R	10	1280	22.3	8.2×10^{-6}	2	(see # 922)
⟶	10	1250		7.9×10^{-6}	2	Di+V
821	20	1230	21.2	1.9×10^{-6}	2	Di+V
657	20	1240	22.4	2.0×10^{-6}	2	Di+(L)+V
661	20	1250	24.8	2.0×10^{-6}	2	Di+L+V
669	20	1250	35.9	2.0×10^{-6}	14	Di+L+V
659	20	1260	30.0	2.1×10^{-6}	2	Di+L+V
824	27.5	1180	20.9	5.9×10^{-7}	0.5	Di+V
826	27.5	1190	27.3	6.1×10^{-7}	0.5	Di+V
823	27.5	1200	31.6	6.3×10^{-7}	0.5	Di+V
1214	27.5	1210	18.5	6.5×10^{-7}	0.5	Di+V
822	27.5	1220	30.9	6.7×10^{-7}	0.5	Di+L+V
793	27.5	1230	27.6	6.9×10^{-7}	0.5	Di+L+V
802	27.5	1240	31.3	7.1×10^{-7}	0.5	Di+L+V
1215R	27.5	1220	22.3	6.9×10^{-7}	0.5	(see # 822)
⟶	27.5	1205		6.4×10^{-7}	0.5	Di+V

Table 1—*Continued*

Run #	P kbar	T °C	H_2O loaded wt%	$X^V_{H_2}$	Duration h	Results
NNO Buffer						
1027	7.5	1260	17.5	2.4×10^{-3}	3	Di+V
984	10	1210	15.1	1.5×10^{-3}	3	Di+V
972	10	1230	20.1	1.6×10^{-3}	3	Di+V
973	10	1240	13.3	1.6×10^{-3}	3	Di+V
976	10	1250	16.0	1.6×10^{-3}	2	Di+V
980	10	1260	18.0	1.6×10^{-3}	4	Di+L+V
1030	20	1220	17.9	3.1×10^{-4}	3	Di+V
1026	20	1230	19.0	3.2×10^{-4}	3	Di+V
1031	20	1240	19.8	3.3×10^{-4}	3	Di+(L)+V
1032	27.5	1190	16.8	8.6×10^{-5}	3	Di+V
1028	27.5	1200	19.5	8.9×10^{-5}	3	Di+L+V
WM Buffer						
680	7.5	1270	18.9	1.0×10^{-3}	2	Di+V
684	7.5	1280	21.0	2.9×10^{-3}	2	Di+L+V
643	10	1250	19.3	1.0×10^{-3}	2	Di+V
647	10	1260	17.9	2.9×10^{-3}	2	Di+V
655	10	1260	18.3	2.9×10^{-3}	4	Di+V
646	10	1270	20.3	1.6×10^{-2}	2	Di+(L)+V
653	10	1270	21.3	1.6×10^{-2}	4	Di+L+V
649	10	1280	20.4	1.6×10^{-2}	2	Di+L+V
673	20	1240	25.1	1.0×10^{-3}	2	Di+V
672	20	1250	26.1	2.8×10^{-3}	2	Di+L+V
IW Buffer						
762	7.5	1280	19.2	0.42	0.5	Di+V
767	7.5	1290	20.1	0.42	0.5	Di+V
769	7.5	1300	28.3	0.42	0.5	Di+V
770	7.5	1310	21.9	0.41	0.5	Di+L+V
1188r	7.5	1310	18.3	0.41	0.5	(see # 770)
⟶	7.5	1295	18.3	0.42	0.5	Di+L+V
687	10	1270	27.5	0.39	2	Di+V
738	10	1290	22.3	0.39	2	Di+V
772	10	1290	23.5	0.39	0.5	Di+V
746	10	1300	24.7	0.38	2	Di+L+V
771	10	1300	30.3	0.38	0.5	Di+L+V
745	10	1310	17.8	0.38	2	L+V
742	10	1330	20.2	0.38	2	Di+L+V
1191R	10	1300	18.6	0.38	0.5	(see # 771)
⟶	10	1285		0.39	0.5	Di+V
760	20	1240	23.5	0.28	2	Di+V
773	20	1250	15.0	0.28	0.5	Di+V
774	20	1270	16.9	0.28	0.5	Di+V
783	20	1280	27.3	0.28	0.5	Di+L+V
777	20	1290	18.9	0.28	0.5	Di+L+V
780	20	1290	24.7	0.28	0.5	Di+L+V
779	20	1300	22.5	0.28	0.5	Di+L+V
778	20	1310	13.4	0.28	0.5	Di+L+V
1210	24	1280	21.2	0.24	0.5	Di+V
1212	24	1290	18.1	0.24	0.5	Di+V
1211	24	1300	18.7	0.24	0.5	Di+L+V
1203	27.5	1200	21.7	0.23	0.5	Di+V
1193	27.5	1240	17.1	0.23	0.5	Di+V
1195	27.5	1270	18.8	0.23	0.5	Di+V
1200	27.5	1290	20.1	0.23	0.5	Di+V
1204	27.5	1300	20.3	0.23	0.5	Di+V
1206	27.5	1310	19.3	0.23	0.5	Di+L+V
1201	27.5	1320	19.7	0.23	0.5	Di+L+V
1207R	27.5	1320	20.2	0.23	0.5	(see #1201)
⟶	27.5	1295		0.23	0.5	Di+V
1216	30	1300	16.3	0.21	0.5	Di+V
1209	30	1310	22.4	0.21	0.5	Di+L+V
1208	30	1330	22.0	0.22	0.5	Di+L+V

Abbreviations: Di=diopside, L=liquid, V=vapor, R=successful reversal, r=attempted reversal, ( )=trace amount, *=run in outer capsule filled with mechanical buffer of SiO_2. $X^V_{H_2}$ calculated as discussed in text.

ference between the pure H_2O and the HM-buffered curves. The three solidi terminate in critical points, where liquid and vapor become indistinguishable. In the SiO_2-H_2O system, this point (K_2 in Fig. 4) is a critical end-point (Kennedy et al., 1962). However, for the SiO_2-H_2O-H_2 compositions, K_A and K_B are critical points, not critical end-points, as explained by Boettcher (1984). The outrageous shape of the vapor-saturated solidus of SiO_2-H_2O-H_2 (IW) has been tightly constrained by reversal experiments at pressures bracketing each abrupt change in slope.

Discussion

The solidus of silicate-H_2O should be univariant, yet the products of our hypersolidus experiments contain solid + liquid + vapor. This behavior may be caused by the incongruent melting of the silicates, thereby causing a divariant melting interval. However, the same behavior is found in the SiO_2-H_2O system, where there can be no such

Table 2. Experimental results for $NaAlSi_3O_8$-H_2O-H_2

Run #	P kbar	T °C	H_2O loaded wt%	$X^v_{H_2}$	Duration h	Results
Pure H_2O, low albite						
842	5	720	26.0	8.3×10^{-10}	8	Ab+V
810	5	730	24.0	1.1×10^{-9}	8	Ab+L+V
799	5	750	25.0	1.6×10^{-9}	24	Ab+L+V
843	5	775	20.5	2.8×10^{-9}	8	Ab+L+V
849R	5	775	20.3	2.8×10^{-9}	5	(see # 843)
⟶	5	720		8.3×10^{-10}	17	Ab+V
1132R	5	730	16.5	1.1×10^{-9}	8	(see # 810)
⟶	5	720		8.3×10^{-10}	15.5	Ab+V
850	10	680	17.3	1.6×10^{-13}	8	Ab+V
851	10	680	16.9	1.6×10^{-13}	15	Ab+V
856	10	690	20.7	2.6×10^{-13}	24	Ab+V
1025	10	700	44.5	4.0×10^{-13}	8	Ab+L+V
1039	10	700	19.4	4.0×10^{-13}	8	Ab+L+V
853	10	700	18.5	4.0×10^{-13}	20	Ab+L+V
1131R	10	700	19.2	4.0×10^{-13}	8	(see # 853)
⟶	10	690		2.6×10^{-13}	15	Ab+V
836	15	630	25.4	4.4×10^{-30}	7.5	Ab+V
839	15	640	22.2	4.1×10^{-29}	8	Ab+V
809	15	650	31.0	3.3×10^{-28}	8	Ab+L+V
844R	15	650	21.4	3.3×10^{-28}	6.5	(see # 809)
⟶	15	640		4.1×10^{-29}	13	Ab+V
Pure H_2O, high albite						
873	5	720	16.0	8.3×10^{-10}	8	Ab+V
894	5	730	21.0	1.1×10^{-9}	8	Ab+V
893	5	740	17.8	1.3×10^{-9}	14	Ab+L+V
872	10	660	18.2	6.1×10^{-14}	8	Ab+V
867	10	670	35.7	1.0×10^{-13}	8	Ab+V
868	10	680	37.0	1.6×10^{-13}	15	Ab+L+V
895	10	680	20.3	1.6×10^{-13}	25	Ab+L+V
866	10	690	27.5	2.5×10^{-13}	9	Ab+L+V
874	10	690	15.9	2.5×10^{-13}	14	Ab+L+V
881	10	700	20.6	4.0×10^{-13}	19	Ab+L+V
882	10	710	19.7	6.1×10^{-13}	19	(Ab)+L+V
891	15	630	17.5	4.4×10^{-30}	8	Ab+V
883	15	640	21.5	4.1×10^{-29}	8	Ab+L+V
HM Buffer, low albite						
785	5	730	22.7	6.4×10^{-6}	24	Ab+V
816	5	740	16.2	6.6×10^{-6}	22	Ab+V
808	5	740	26.5	6.6×10^{-6}	24	Ab+V
3045	5	750	20.0	6.7×10^{-6}	24	Ab+V
819	5	760	21.5	6.9×10^{-6}	9	Ab+V
817	5	760	23.1	6.9×10^{-6}	7.5	Ab+(L)+V
801	5	770	31.7	7.1×10^{-6}	24	Ab+L+V
1133R	5	770	19.5	7.1×10^{-6}	7.5	(see # 801)
⟶	5	750		6.7×10^{-6}	14	Ab+V
784	10	680	24.8	1.9×10^{-6}	24	Ab+V
857	10	700	23.0	2.0×10^{-6}	8	Ab+V
3026	10	700	20.0	2.0×10^{-6}	24	Ab+V

Table 2—*Continued*

Run #	P kbar	T °C	H_2O loaded wt%	$X^v_{H_2}$	Duration h	Results
855	10	710	21.8	2.1×10^{-6}	5	Ab+L+V
858	10	710	19.6	2.1×10^{-6}	9	Ab+L+V
854	10	730	23.7	2.3×10^{-6}	15	Ab+L+V
1151R	10	710	21.1	2.1×10^{-6}	8	(see # 858)
⟶	10	690		2.0×10^{-6}	14	Ab+V
800	15	660	27.8	5.7×10^{-7}	24	Ab+V
805	15	680	29.3	6.4×10^{-7}	24	Ab+V
818	15	690	23.2	6.7×10^{-7}	24	Ab+L+V
820	15	700	23.0	7.0×10^{-7}	7.5	L+V
807	15	700	29.1	7.0×10^{-7}	24	L+V
1064	16	680	19.6	4.6×10^{-7}	8	Ab+L+V
1052	17	660	18.4	3.7×10^{-7}	8	Ab+V
1063	17	670	20.5	3.9×10^{-7}	8	Ab+L+V
1051	17	680	18.5	4.1×10^{-7}	8	Ab+L+V
NNO Buffer, low albite						
1011	5	740	15.7	1.6×10^{-3}	8	Ab+V
1010	5	750	17.2	1.6×10^{-3}	8	Ab+L+V
1006	5	760	19.5	1.7×10^{-3}	8	Ab+L+V
995	10	700	16.9	4.2×10^{-4}	8	Ab+V
998	10	710	18.3	4.4×10^{-4}	8	Ab+L+V
996	10	720	18.9	4.6×10^{-4}	8	Ab+L+V
997	15	680	17.2	1.1×10^{-4}	8	Ab+V
1000	15	690	19.1	1.2×10^{-4}	8	Ab+L+V
999	15	700	19.4	1.3×10^{-4}	8	Ab+L+V
IW Buffer, low albite						
845	5	750	19.2	0.53	6	Ab+V
846	5	760	17.5	0.53	6	Ab+V
835	5	770	23.5	0.53	6	Ab+L+V
831	5	790	25.8	0.53	6	Ab+L+V
1140R	5	770	18.5	0.53	7.5	(see # 835)
⟶	5	760		0.53	6	Ab+V
1128	10	720	19.1	0.45	8	Ab+V
1129	10	730	17.4	0.44	8	Ab+V
1138	10	740	16.2	0.44	8	Ab+L+V
1139	10	750	18.9	0.43	10	Ab+L+V
828	15	700	25.8	0.36	7.5	Ab+V
834	15	710	28.1	0.36	7.5	Ab+L+V
829	15	720	23.3	0.36	7.5	Ab+L+V
1066	17	680	19.6	0.32	8	Ab+V
1068	17	690	16.2	0.33	8	Ab+L+V
1067	17	700	20.0	0.33	8	Ab+L+V

Abbreviations: Ab=albite, L=liquid, V=vapor, R=successful reversal, r=attempted reversal, ( )=trace amount, $X^v_{H_2}$ calculated as discussed in text.

incongruency, so that this cannot be a general explanation. Alternatively, there may be insufficient H_2O in the capsule to allow the formation of 100% H_2O–saturated liquid. If this were the case, however, there would be no quenched vapor in the run products, contrary to what is observed. Finally, and most probably, we have allowed insufficient time for all of the solid to melt. However, determination of the solidus does not require complete melting, and our reversal experiments verify that our curves represent equilibrium.

The increase in temperature of the vapor-saturated solidi with increasing $X^v_{H_2}$ may largely result from a simple lowering of the $a^v_{H_2O}$, with H_2 acting as as an inert diluent in the vapor. However, several factors indicate that H_2 is soluble in silicate liquids. First, increasing the $X^v_{H_2}$ from $<10^{-10}$ (calculated for pure H_2O) to $\sim10^{-5}$ (calculated for HM-buffered vapor) increases the temperature of the vapor-saturated solidi at a given pressure disproportionately to the calculated decrease in $X^v_{H_2O}$. Second, vapor-saturated solidus temperatures at a given $a^v_{H_2O}$ are lower in the presence of H_2O-H_2 vapors than in the presence of a vapor of either H_2O-CO_2 or H_2O-X, where X is an inert, insoluble diluent, suggesting that H_2 is soluble in these liquids, probably more so than is CO_2. Each of these factors will be discussed in turn.

The difference between the solidus for pure H_2O and that buffered by HM may be caused by the reaction of H_2 with one of the phases. Trace amounts (<0.1 wt%) of H_2O, either as OH groups or as H_2O molecules, have been found in garnets (Aines and Rossman, 1984a), olivine (Beran and Putnis, 1983), and quartz (Aines and Rossman, 1984b; Aines et al., 1984), whereas there is no evidence for molecular H_2 in these minerals. Because H_2O dissolved in the solid stabilizes the solid + vapor assemblage relative to liquid, dehydration of the solid resulting from lowered $a^v_{H_2O}$ stabilizes the liquid and lowers the temperature of the vapor-saturated solidus. However, this effect would decrease solidus temperatures with increasing $X^v_{H_2}$, opposite to what is observed.

Alternatively, if the calculated values of $X^v_{H_2}$ for the HM

Table 3. Experimental results for SiO_2-H_2O-H_2

Run #	P kbar	T °C	H_2O loaded wt%	$X^v_{H_2}$	Duration h	Results
Pure H_2O						
1086	5	1050	19.9	2.5×10^{-7}	2	Qz+V
1042	5	1060	19.9	2.8×10^{-7}	2	Qz+L+V
1159R	5	1060	18.2	2.8×10^{-7}	2	(see #1042)
⟶	5	1050		2.5×10^{-7}	2	Qz+V
1037	7	1050	17.4	8.4×10^{-8}	2	Qz+V
1040	7	1060	18.0	9.7×10^{-8}	2	Qz+L+V
1038	9	1015	15.7	1.1×10^{-8}	2	Qz+V
1034	9	1030	17.4	1.4×10^{-8}	2	Qz+V
1035	9	1040	17.0	1.7×10^{-8}	2	Qz+V
1033	9	1050	12.0	2.0×10^{-8}	2	Qz+L+V
1058R	9	1050	15.7	2.0×10^{-8}	2	(see #1033)
⟶	9	1040		1.7×10^{-8}	2	Qz+V
HM Buffer						
1092	5	1060	17.4	1.2×10^{-5}	2	Qz+V
1097	5	1080	18.5	1.3×10^{-5}	2	Qz+V
1099	5	1090	17.4	1.3×10^{-5}	2	Qz+V
1106	5	1110	19.7	1.3×10^{-5}	2	Qz+V
1113	5	1120	19.2	1.3×10^{-5}	2	Qz+L+V
1107	5	1130	17.0	1.4×10^{-5}	2	Qz+L+V
1161r	5	1120	21.3	1.3×10^{-5}	2	(see #1113)
⟶	5	1110		1.3×10^{-5}	2	Qz+L+V
1166R	5	1120	16.8	1.3×10^{-5}	2	(see #1113)
⟶	5	1100		1.3×10^{-5}	4	Qz+V
1116	7	1050	18.2	8.8×10^{-6}	2	Qz+V
1098	7	1070	18.8	9.1×10^{-6}	2	Qz+V
1100	7	1070	19.1	9.1×10^{-6}	4	Qz+V
1101	7	1080	22.2	9.3×10^{-6}	2	Qz+V
1110	7	1090	19.2	9.5×10^{-6}	2	Qz+V
1105	7	1100	19.5	9.6×10^{-6}	2	Qz+L+V
1123	9	1060	18.3	6.6×10^{-6}	2	Qz+V
1127	9	1070	23.3	6.7×10^{-6}	2	Qz+V
1117	9	1080	20.8	6.8×10^{-6}	2	Qz+L+V
IW Buffer						
1087	5	1160	21.4	0.48	2	Qz+V
1089	5	1170	16.5	0.48	2	Qz+L+V
1060	7	1070	16.7	0.46	2	Qz+V
1061	7	1090	21.3	0.46	2	Qz+V
1059	7	1110	21.3	0.46	2	Qz+V
1073	7	1130	18.0	0.45	2	Qz+V
1074	7	1140	18.8	0.45	2	Qz+V
1075	7	1150	20.2	0.45	2	Qz+V
1072	7	1160	19.6	0.45	2	Qz+L+V
1071	7	1180	14.9	0.45	2	Qz+L+V
1170	7	1200	19.7	0.45	2	L+V
1076	9	1150	20.9	0.43	2	Qz+V
1080	9	1160	19.9	0.43	2	Qz+L+V
1079	9	1170	18.4	0.43	2	(Qz)+L+V
1141R	9	1160	14.2	0.43	2	(see #1080)
⟶	9	1150		0.43	2	Qz+V
1122	10.5	1110	19.9	0.41	2	Qz+V
1135	10.5	1120	21.2	0.41	2	L+V
1121	10.5	1130	21.7	0.41	2	L+V
1146r	10.5	1120	21.4	0.41	2	(see #1135)
⟶	10.5	1110		0.41	2	L+V
1156R	10.5	1120	18.5	0.41	2	(see #1135)
⟶	10.5	1100		0.41	2	Qz+V
1104	12	1090	14.3	0.39	2	Qz+V
1109	12	1100	20.6	0.39	2	Qz+V
1102	12	1110	17.2	0.39	2	Qz+L+V
1093	12	1120	17.3	0.39	2	Qz+L+V
1090	12	1130	21.7	0.39	2	Qz+L+V
1148	15	1100	18.1	0.36	2	Qz+V
1088	15	1110	18.7	0.36	2	(Qz)+L+V
1085	15	1120	19.9	0.36	2	(Qz)+L+V
1082	15	1140	19.2	0.36	2	L+V
1081	15	1160	19.8	0.36	2	L+V
1136r	15	1110	18.7	0.36	2	(see #1088)
⟶	15	1100		0.36	2	L+V
1147R	15	1110	16.3	0.36	2	(see #1088)
⟶	15	1090		0.36	2	Qz+V
1119	17.5	1050	20.3	0.33	2	Qz+V
1120	17.5	1060	18.9	0.33	2	Qz+L+V
1118	17.5	1070	18.9	0.33	2	Qz+L+V
1144R	17.5	1060	20.2	0.33	2	(see #1120)
⟶	17.5	1050		0.33	2	Qz+V
1095	20	1050	20.4	0.30	2	Qz+V
1096	20	1060	17.1	0.30	2	Qz+L+V
1091	20	1070	20.6	0.30	2	Qz+L+V
1145r	20	1060	22.0	0.30	2	(see #1096)
⟶	20	1050		0.30	2	Qz+L+V
1155R	20	1060	19.1	0.30	2	(see #1096)
⟶	20	1040		0.30	2	Qz+V
1103	25	1000	18.8	0.24	2	Qz+V
1124	25	1020	19.5	0.24	2	Qz+V
1125	25	1030	19.9	0.24	2	Qz+V
1108	25	1040	20.1	0.24	2	Qz+L+V
1112	25	1060	21.5	0.25	2	Qz+L+V
1114	25	1070	18.1	0.25	2	Qz+L+V
1111	25	1080	20.9	0.25	2	Qz+L+V
1176	27.5	1020	21.5	0.22	2	Qz+V
1177	27.5	1030	18.8	0.22	2	Qz+V
1174	27.5	1040	20.2	0.22	2	Qz+L+V
1173	27.5	1060	20.9	0.22	2	Qz+L+V
1179R	27.5	1040	18.6	0.22	2	(see #1174)
⟶	27.5	1020		0.22	2	Qz+V
1162	30	1020	17.8	0.20	2	Qz+F
1163	30	1040	20.4	0.20	2	Qz+F
1164	30	1060	17.4	0.20	2	Qz+F
1168	30	1080	20.1	0.20	2	Qz+F
1169	30	1100	20.1	0.20	2	Qz+F
1180	35	1100	20.5	0.17	2	Ct+F
1182	35	1120	18.9	0.17	1	Ct+F
1181	35	1140	22.4	0.17	1	Ct+F
1183	35	1160	17.3	0.17	1	Ct+F

Abbreviations: Qz=quartz, Ct=coesite, L=liquid, V=vapor, F=supercritical fluid, R=successful reversal, r=attempted reversal, ( )=trace amount, $X^v_{H_2}$ calculated as discussed in text.

buffer are systematically too low because of the uncertainties discussed previously in the section on Calculation of Vapor Composition, the difference between pure-H_2O and HM-buffered solidi may simply result from the difference in $X^v_{H_2}$ with H_2 acting as an inert diluent. However, this requires that the combined uncertainties in the calculation of the vapor composition would change $a^v_{H_2}$ by a factor of 10^{+4}, which appears to be unrealistic.

Of great interest is the possibility that the difference between the vapor-saturated solidus for pure H_2O and that buffered by HM results from solubility of H_2 in the liquids. For example, H_2 may associate with H_2O in the liquid, increasing the molar volume of the H_2O-H_2 complex in the liquid, decreasing $a^l_{H_2O}$ and stabilizing the solid + vapor assemblage to higher pressures and temperatures. H_2 could also lower the $a^l_{H_2O}$ by forming bonds with ions in the liquid or by occupying sites as molecular H_2 that otherwise would be filled by H_2O. The distortion of the liquid caused by H_2 molecules occupying sites that are appropriate for H_2O molecules would increase the free energy of the liquid and thereby increase melting temperatures. One possible reaction is to form Si–H bonds in the liquid. Infrared evidence for Si–H bonds was obtained by Faile and Roy (1970) in SiO_2 glass containing 2 mol% H_2 that had been subjected to gamma-radiation and a neutron flux. They postulated that the irradiation provided the energy to break H–H and Si–O–Si bonds to form Si–O–H and Si–H bonds. Perhaps the higher temperatures in our study provided the necessary activation energy to form Si–H bonds.

Would formation of Si–H bonds strengthen or weaken neighboring bonds? If Si–H bonds strengthen neighboring Si–O bonds, it would be more difficult to locally break a Si–O–Si bridge to form Si–O–H groups. Alternatively, if

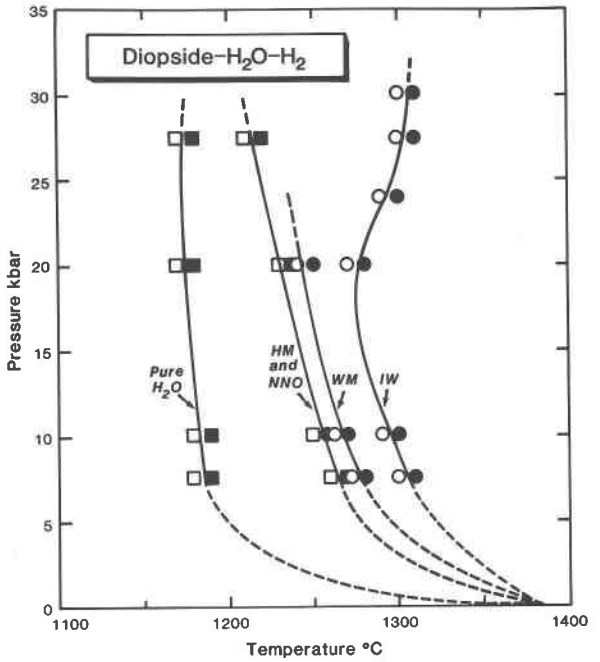

Fig. 1. Pressure-temperature projection of the vapor-saturated solidi of diopside + vapor for various values of the activity of hydrogen in the vapor ($a^v_{H_2}$). Closed symbols represent diopside + liquid + vapor; open symbols are diospide + vapor. Values of $a^v_{H_2}$ are buffered by pure H_2O, hematite-magnetite-H_2O (HM), nickel–nickel oxide–H_2O (NNO), wüstite-magnetite-H_2O (WM), and iron-wüstite-H_2 (IW). Where determined, the NNO-buffered solidus coincides with the HM-buffered solidus.

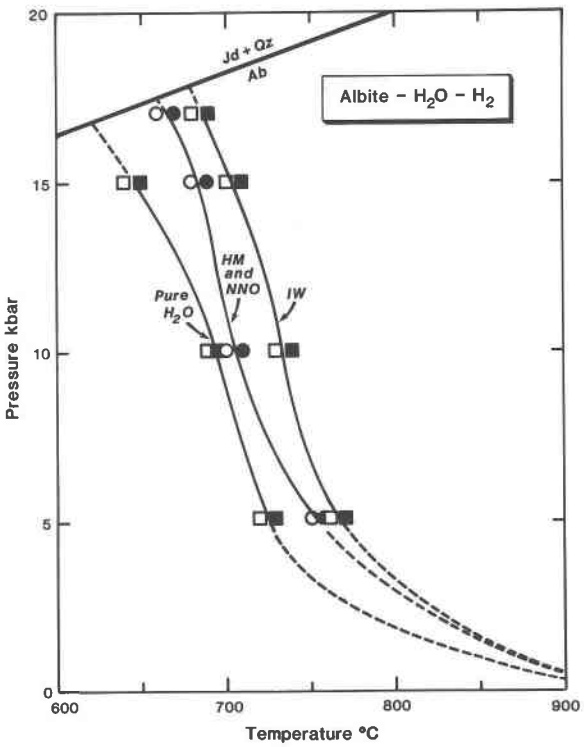

Fig. 2. Pressure-temperature projection of the vapor-saturated solidi of albite + vapor for various values of $a^v_{H_2}$. Closed symbols represent albite + liquid + vapor; open symbols are albite + vapor. Values of $a^v_{H_2}$ are buffered by the same assemblages as in Fig. 1. Where determined, the NNO-buffered solidus coincides with the HM-buffered solidus. The albite = jadeite + quartz reaction is from Boettcher and Wyllie (1968).

Si–H bonds weaken the Si–O bonds of those Si cations, those bonds would preferentially react with H_2O to form Si–O–H groups, effectively ordering the Si–O–H groups in the liquid. The resulting decrease in entropy would increase the free energy of the liquid and increase melting temperatures. Either way, disruption of the framework of the silicate liquid could lead to less favorable conditions for Si–O–H bonding than in the absence of H_2, thereby decreasing $a^l_{H_2O}$ and increasing solidus temperatures.

One possible explanation of the difference between the pure-H_2O and the HM-buffered solidi of $CaMgSi_2O_6$-H_2O-H_2 and of $NaAlSi_3O_8$-H_2O-H_2 is the differing extent of incongruent solubility of silicate components in the vapor as $X^v_{H_2}$ increases. With extensive incongruent solubility of the crystalline phase in the vapor, the residual solid departs from $NaAlSi_3O_8$ or $CaMgSi_2O_6$ composition and melts at a different temperature. However, the same effect is seen in SiO_2-H_2O-H_2, where there is only one silicate component and no possibility of incongruent solution of silicates in the vapor.

Comparison of the effects of H_2 on the vapor-saturated solidi with those of an inert diluent and with those of CO_2 provide insight into the solubility of H_2 in these silicate liquids. We calculated the phase relations for silicate-H_2O-X using thermochemical data, activity coefficients for the components in the vapor provided by the MRK equation, and the assumption that X was completely insoluble in the liquids. The data for silicate-H_2O-CO_2 were taken from the literature.

Vapor-saturated solidi of $CaMgSi_2O_6$-H_2O and $CaMgSi_2O_6$-H_2O-X (Fig. 5) were calculated using the model of Eggler and Burnham (1984). To calculate the solidus, this model required the temperature of the solidus of $CaMgSi_2O_6$-H_2O at one pressure, as determined by Eggler and Rosenhauer (1978). If this temperature is revised downward to agree with our data on the solidus of $CaMgSi_2O_6$-H_2O, the calculated solidus becomes lower in temperature than the experimental solidus, with the difference between the two increasing from ~20°C at 10 kbar to ~100°C at 27.5 kbar. Without a better thermodynamic model for the phase relations in $CaMgSi_2O_6$-H_2O, it is impossible to say if H_2 is dissolving in the liquid. However, comparing the vapor-saturated solidus of $CaMgSi_2O_6$-H_2O-CO_2 and that of $CaMgSi_2O_6$-H_2O-H_2 (IW) (Fig. 6) suggests that below ~15 kbar, H_2 and CO_2 have similar effects on the melting temperatures at $X^v_{H_2O} \approx 0.70$. Above this pressure, the solidus of $CaMgSi_2O_6$-H_2O-H_2 (IW) increases in temperature with increasing pressure, whereas the solidus of $CaMgSi_2O_6$-H_2O-CO_2 continues to decrease in temperature with increasing pressure. This difference may result from an increase in the solubility of CO_2 or

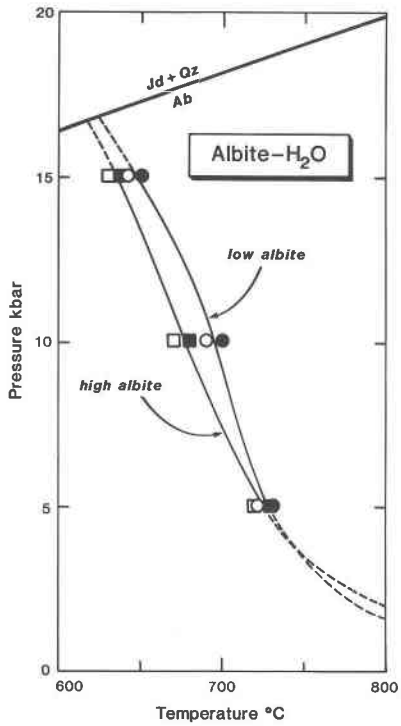

Fig. 3. Pressure-temperature projection of the vapor-saturated solidi of high albite + vapor and low albite + vapor in the system $NaAlSi_3O_8$-H_2O. Closed symbols represent albite + liquid + vapor; open symbols are albite + vapor.

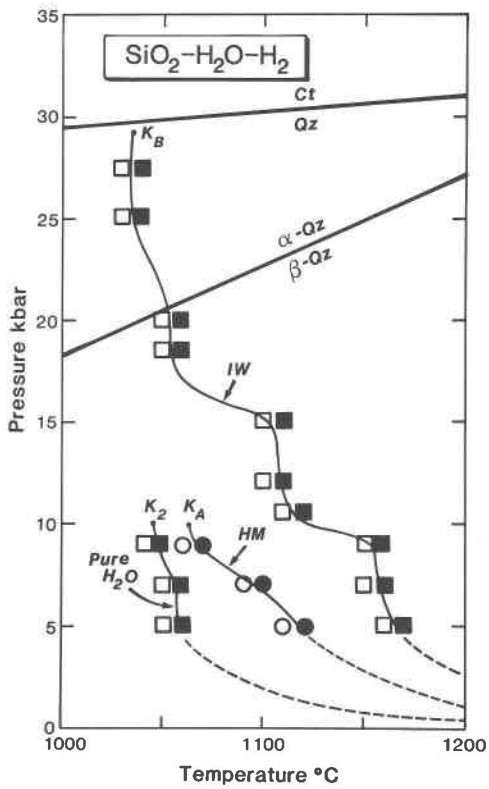

Fig. 4. Pressure-temperature projection of the vapor-saturated solidi of quartz + vapor for various values of $a^v_{H_2}$. Closed symbols represent quartz + liquid + vapor; open symbols are quartz + vapor. Values of $a^v_{H_2}$ are buffered by pure H_2O, hematite-magnetite-H_2O (HM) and iron-wüstite-H_2O (IW). The α–β quartz transition is from Cohen and Klement (1967), and Bohlen and Boettcher (1982) determined the quartz = coesite transition to 1000°C, here extrapolated to higher temperatures. K_2 is a critical end-point in the system SiO_2-H_2O. K_A and K_B are critical points for SiO_2-H_2O-H_2.

H_2O or both in the $CaMgSi_2O_6$-H_2O-CO_2 liquid with increasing pressure, or a decrease in the solubility of H_2 or H_2O or both in the $CaMgSi_2O_6$-H_2O-H_2 liquid with increasing pressure. The proposed pressure-induced structural changes in these liquids cannot be defined without more data on the solubility of the volatile components; this will be hard to acquire because these hydrous liquids do not quench to glass, but rather to an intergrowth of quench crystals and glass, complicating analysis of the run products. Experiments at temperatures well above the liquidus quench to glass, but temperature-induced structural degradation of the liquids renders the results less useful (Boettcher et al., 1982).

The temperature of the vapor-saturated solidus of $NaAlSi_3O_8$-H_2O-H_2 (IW) is consistently lower at all pressures than the solidus of $NaAlSi_3O_8$-H_2O-CO_2 (Fig. 7) or that of $NaAlSi_3O_8$-H_2O-X (Fig. 8), calculated using the data of Burnham (1979). The difference between the experimental and calculated solidi (Fig. 8) is ~175°C, much larger than the difference between the calculated and experimental solidi for $NaAlSi_3O_8$-H_2O (~30°C), suggesting that H_2 as well as H_2O dissolves in the liquid. Further, the difference between the solidus of $NaAlSi_3O_8$-H_2O-H_2 and that of $NaAlSi_3O_8$-H_2O-CO_2 (Fig. 7) suggests that the solubility of H_2 is higher in the liquid than is that of CO_2, or that the activity coefficients for H_2 are greater than those for CO_2, or that the calculated values for $X^v_{H_2O}$ for the IW buffer are too low. Data on H_2O-CO_2 mixtures suggest that activity coefficients in these vapors are approximately unity (Bohlen et al., 1982, 1983; Kerrick and Jacobs, 1981; Boettcher, 1984) and that they may be modeled, to a first approximation, by a variant of the MRK equation of state (Holloway, 1977; Kerrick and Jacobs, 1981). The data available on H_2O-H_2 mixtures (Shaw, 1963) are consistent with activity coefficients for both components on the order of unity. As discussed previously, the calculated $X^v_{H_2O}$ may be incorrect, but they would have to be too small, instead of too large, as would be required for the HM-buffered vapors. If these calculated values for $X^v_{H_2O}$ are correct, then the difference in the solidi must reflect the higher solubility of H_2 relative to CO_2 in the liquid.

The experimentally determined solidus of SiO_2-H_2O-H_2 (IW) lies consistently at lower temperature for a given pressure than does the corresponding solidus of SiO_2-H_2O-CO_2 (Fig. 9) or that of SiO_2-H_2O-X (Fig. 10), modified from Boettcher (1984), for the same $a^v_{H_2O}$. The difference in temperature increases with increasing pressure, imply-

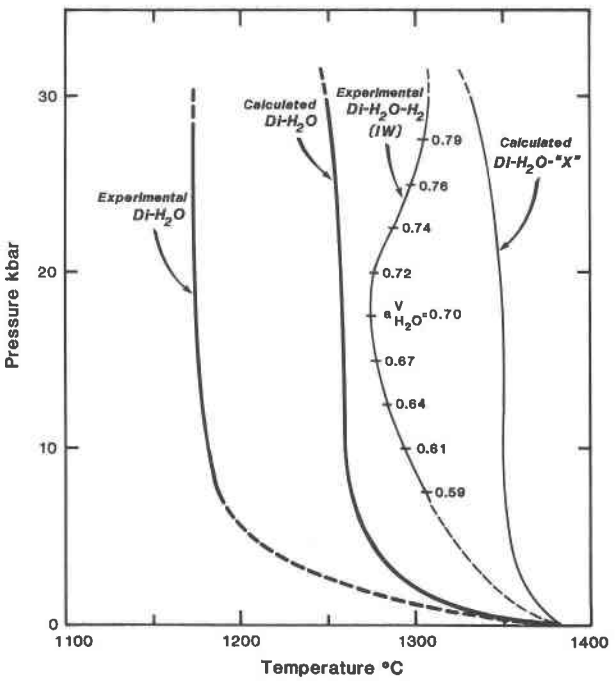

Fig. 5. Pressure-temperature projection of experimentally determined and calculated vapor-saturated solidi of diopside + vapor. Note the difference between the calculated and experimental $CaMgSi_2O_6$-H_2O solidi. The solidus of $CaMgSi_2O_6$-H_2O-H_2 (IW) is shown with the values of aH_2O along the curve. The $CaMgSi_2O_6$-H_2O-X solidus was calculated assuming an inert component in the vapor and the same $a^v_{H_2}$ as in the experimental curve at any given pressure.

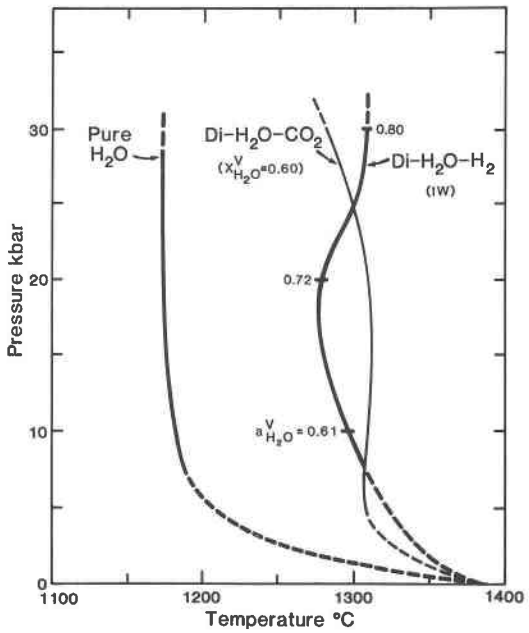

Fig. 6. Pressure-temperature projection of the solidus of $CaMgSi_2O_6$-H_2O-H_2 (IW) and that of $CaMgSi_2O_6$-H_2O-CO_2 with $X^v_{H_2O}$ fixed at 0.60. Values of $a^v_{H_2O}$ along the $CaMgSi_2O_6$-H_2O-H_2 (IW) solidus are shown by the numbers along the curve. The solidus of $CaMgSi_2O_6$-H_2O-CO_2 is from Eggler and Rosenhauer (1978).

ing a concomitant increase in the solubility of H_2. Compared to the $NaAlSi_3O_8$-containing systems, the SiO_2-containing systems show a greater difference in temperature between the solidus for SiO_2-H_2O-H_2 (IW) and the equivalent SiO_2-H_2O-CO_2 solidus, which may be a real difference in the solubility of H_2 or an artifact of comparing such different systems in this fashion. Nevertheless, the explanation offered above for the $NaAlSi_3O_8$-bearing systems, that H_2 is more soluble than is CO_2 at low $X^v_{H_2O}$, may also be appropriate for SiO_2-H_2O-H_2 and SiO_2-H_2O-CO_2.

The abrupt changes in slope of the vapor-saturated solidus of SiO_2-H_2O-H_2 (IW) may be explained by pressure-induced transformations in either the liquid or the vapor. However, we favor a mechanism involving a decrease in the free energy of the liquid caused by structural changes that increase the solubility of H_2O and/or H_2. In any case, the abruptness of the changes in slope of the solidus suggest that there must be important structural changes in the liquid with increasing pressure, making the calculation of melting equilibria, even in this simple case, hazardous unless complemented by tightly constrained experimental determinations.

The difference in behavior of H_2 and CO_2 may also be seen in their respective effects on the critical end-point in SiO_2-H_2O. Dilution of the vapor phase with ~30 mol% H_2 shifts the critical point from ~10 kbar to ~29 kbar, whereas only 5 mol% CO_2 increases the pressure of the critical point to ~26 kbar. This difference suggests that the liquid and vapor in SiO_2-H_2O change character less when diluted by H_2 than when diluted by CO_2. The solubility of both H_2O and H_2 in the liquid must be higher than the solubility of H_2O and CO_2 under the same conditions, and the solubility of SiO_2 in the vapor must be greater in a H_2O-H_2 vapor than in a H_2O-CO_2 vapor.

Our results reveal that experimental apparatus must be calibrated to determine their intrinsic f_{H_2}. Such differences may explain why, for example, the vapor-saturated solidus for $CaMgSi_2O_6$-H_2O determined by Eggler and Rosenhauer (1978) in an internally heated pressure vessel lies between our solidus for pure-H_2O and that for HM-buffered vapor below 10-kbar pressure. Their internally heated pressure vessel had an argon pressure medium and an intrinsic f_{O_2} near the NNO buffer. If the argon contained some H_2O, the f_{H_2} would be lower than that for hydrous vapor in equilibrium with NNO, possibly lower than the f_{H_2} for vapors in equilibrium with HM, which would be consistent with our results. At higher pressures, Eggler and Rosenhauer (1978) used a solid-media high-pressure apparatus with intrinsic f_{O_2} slightly lower than the HM buffer (Eggler et al., 1974), and their solidus above 10 kbar is consistent with the vapor having an f_{H_2} between that of vapors buffered by HM and IW based on our results.

Bohlen et al. (1982) discussed discrepant data for vapor-saturated solidi in the system $NaAlSi_3O_8$-H_2O. Bohlen et

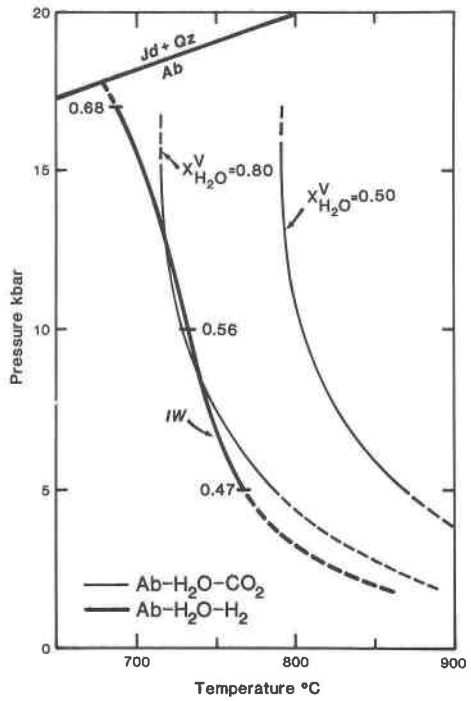

Fig. 7. Pressure-temperature projection of the solidus of $NaAlSi_3O_8$-H_2O-H_2 (IW) and the solidi of $NaAlSi_3O_8$-H_2O-CO_2 with various values of $X^v_{H_2O}$. Values of $a^v_{H_2O}$ along the $NaAlSi_3O_8$-H_2O-H_2 (IW) solidus are shown by the numbers along the curve. Each solidus in the system $NaAlSi_3O_8$-H_2O-CO_2 (Bohlen et al., 1982) has a fixed value of $X^v_{H_2O}$ given by the number along the curve.

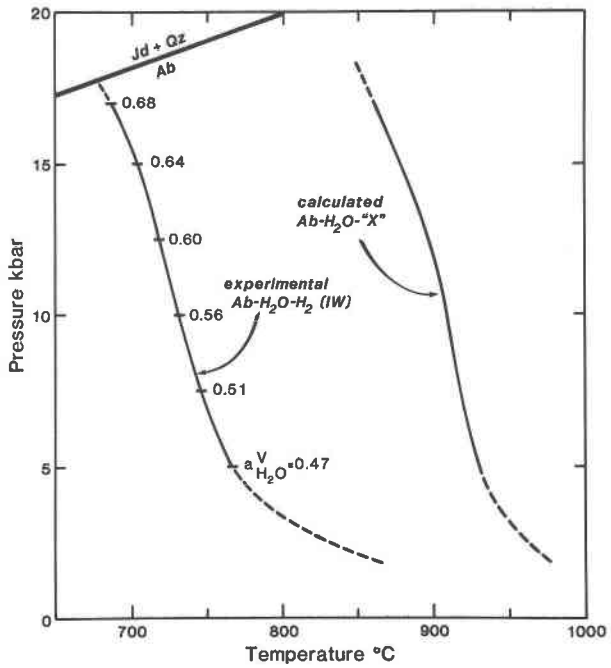

Fig. 8. Pressure-temperature projection of experimentally determined and calculated vapor-saturated solidi of albite + vapor. The experimental curve is for $NaAlSi_3O_8$-H_2O-H_2 (IW), with the $a^v_{H_2O}$ indicated by the numbers along the solidus. The $NaAlSi_3O_8$-H_2O-X solidus is calculated assuming an inert diluent in the vapor and the same $a^v_{H_2O}$ as for the experimental curve at a given pressure.

al. bracketed the solidus at 10 and 15 kbar at 670–680°C and 635–645°C, respectively. Boettcher and Wyllie (1969) had 10- and 15-kbar brackets at 680–690°C and 650–660°C, respectively. W. C. Luth et al. (1964) reported brackets of 10.3 kbar, 695°C and 10.0 kbar, 720°C. Morse (1970) bracketed the solidus at 5 kbar at 758 ± 3°C in both cold-seal and internally heated apparatus. His results are dissonant with ours (Fig. 2) and with those obtained previously by us in piston-cylinder and gas-pressure apparatus (see Bohlen et al., 1982) and with the values of Tuttle and Bowen (1958) extrapolated from 4 kbar. The differences between these results are probably caused by differences in the f_{H_2} in the various apparatus. Bohlen et al. used an "anhydrous" solid-media pressure cell that would have the lowest f_{H_2} (Boettcher et al., 1981). Boettcher and Wyllie (1969) used a talc furnace assembly, with a higher f_{H_2}, around NNO, resulting from the H_2O released during dehydration of the talc. The intrinsic f_{O_2} of both apparatus used by Morse was near the NNO buffer (Morse, pers. comm., 1984), and his results agree with our results for $NaAlSi_3O_8$-H_2O-H_2 (NNO) as well as with our results for $NaAlSi_3O_8$-H_2O-H_2 (HM).

Comparing our results for the system SiO_2-H_2O-H_2 with earlier work, our 9-kbar solidus for SiO_2-H_2O-H_2 (HM) is bracketed between the solidus of Kennedy et al. (1962) and that of Stewart (1967). Both Stewart and Kennedy et al. used internally heated pressure vessels with argon pressure media, yet the solidus determined by Stewart is ~40°C lower than the solidus determined by Kennedy et al. Stewart used the internally heated pressure vessel at the Geophysical Laboratory in Washington, D.C., the same apparatus used by Eggler and Rosenhauer (1978) and Morse (1970), with a pressure medium of light-bulb-grade argon (Morse, pers. comm., 1984). The results of all of these studies suggest an f_{H_2} for this apparatus between that for a vapor of pure H_2O and that for a vapor buffered by HM. The higher results obtained by Kennedy et al. may be explained by a higher f_{H_2} in their apparatus generated by a higher $X^v_{H_2O}$ in the pressure medium. Conceivably, many inconsistent phase-equilibrium data may be reconciled when the f_{H_2} of the experimental apparatus is considered.

The effect of f_{H_2} in these melting experiments has many petrologic applications other than illustrating that f_{H_2} is an important factor in phase-equilibrium experiments. Recent measurements of intrinsic f_{O_2} in xenoliths from the upper mantle (Arculus and Delano, 1981) were interpreted as indicating that parts of the upper mantle have an f_{O_2} more reducing than IW. The presence of native iron in granulite xenoliths from a kimberlite is further evidence for conditions of low f_{O_2} in regions of the continental lower crust and upper mantle (Haggerty and Toft, 1985). Under these conditions, the melting of silicates in the presence of a hydrous vapor phase would occur at higher temper-

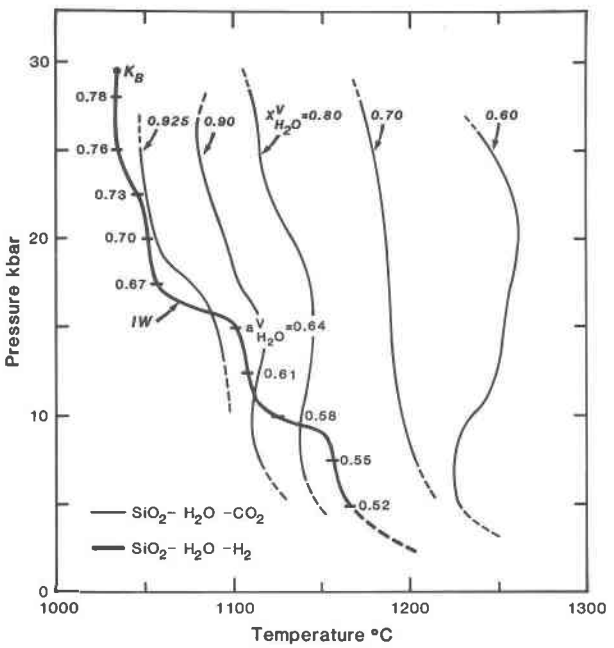

Fig. 9. Pressure-temperature projection of the solidus of SiO_2-H_2O-H_2 (IW) and the solidi of SiO_2-H_2O-CO_2 with various values of $X^v_{H_2O}$. Values of $a^v_{H_2O}$ along the SiO_2-H_2O-H_2 (IW) solidus are shown by the numbers along the curve. Each solidus in the system SiO_2-H_2O-CO_2 (Boettcher, 1984) has a fixed value of $X^v_{H_2O}$ given by the number along the curve.

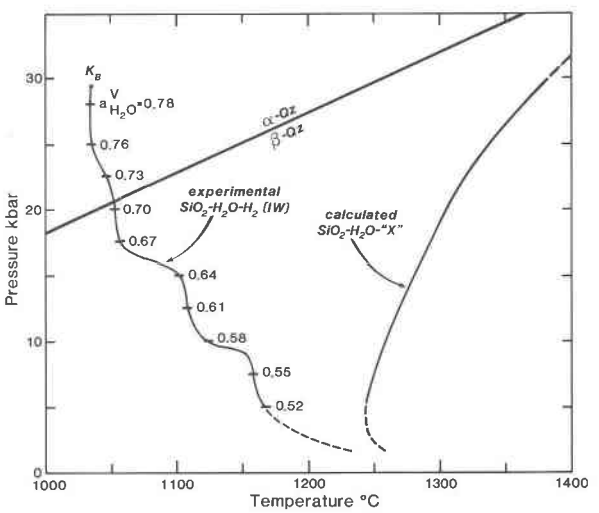

Fig. 10. Pressure-temperature projection of experimentally determined and calculated vapor-saturated solidi of quartz + vapor. The experimental curve is for SiO_2-H_2O-H_2 (IW), with the numbers along the solidus representing the $a^v_{H_2O}$. The SiO_2-H_2O-X solidus is calculated assuming an inert diluent in the vapor, with the same $a^v_{H_2O}$ as for the experimental curve at any given pressure.

atures than in the presence of pure H_2O, but at lower temperatures than in the presence of a H_2O-CO_2 vapor with the same $a^v_{H_2O}$. Further, under these reducing conditions, fluids in the upper mantle would be a mixture of H_2O and H_2, carrying smaller amounts of dissolved silicates than would pure H_2O, thereby lessening the effect of metasomatizing fluids on changing the chemistry of the material with which they interact. Increasing $X^v_{H_2}$ may also affect partitioning of trace elements between solid and fluid phases, altering the trace-element characteristics of the metasomatized rocks.

The lower solubility of H_2 in silicate liquids relative to H_2O is also significant for models of degassing of the Earth and migration of H_2 in the mantle. H_2 is less likely to trigger melting than is H_2O, and, unlike H_2O, H_2 cannot react extensively with solid phases in the mantle, suggesting that H_2 will not become trapped in either a solid phase or a silicate liquid, and it may escape from the mantle (Welhan and Craig, 1979) or provide some control on the oxidation state of the mantle.

In the crust, most igneous rocks equilibrated at values of f_{O_2} near those of the QFM buffer. In the presence of a hydrous vapor buffered by QFM, melting would occur at temperatures as much as 80°C higher than the vapor-saturated solidus in the presence of pure H_2O. Furthermore, under such relatively reducing conditions in the crust, the low solubility of silicates in the vapor with relatively high values of $X^v_{H_2}$ will diminish the metasomatizing ability of the vapor. Zones of intense alteration probably occur only under very oxidizing conditions, and this is consonant with the mineralogy of many pegmatites, where fluid-phase metasomatism commonly is pervasive and extensive.

Acknowledgments

Discussions with Ed Stolper and Bruce Bathurst have been most helpful. Reviews by Stolper and David Eggler are appreciated. Scott Boettcher, Steve Chambers, and Les Faus assisted with the conception and conductions of the experiments. We are indebted to J. M. Christie and R. Coleman for providing the quartz and albite. The National Science Foundation supported this research with grants EAR78-16413, EAR82-10695, and EAR83-06410 to Boettcher and with a Graduate Fellowship to Luth.

References

Aines, R.D., and Rossman, G.R. (1984a) The hydrous component in garnets: pyralspites. American Mineralogist, 69, 1116–1126.

——— (1984b) Water in minerals? A peak in the infrared. Journal of Geophysical Research, 89, 4059–4071.

Aines, R.D., Kirby, S.H., and Rossman, G.R. (1984) Hydrogen speciation in synthetic quartz. Physics and Chemistry of Minerals, 11, 204–212.

Arculus, R.J., and Delano, J.W. (1981) Intrinsic oxygen fugacity measurements: techniques and results for spinels from upper mantle peridotites and megacryst assemblages. Geochimica et Cosmochimica Acta, 45, 899–913.

Beran, A., and Putnis, A. (1983) A model of the OH positions in olivine, derived from infrared-spectroscopic investigations. Physics and Chemistry of Minerals, 9, 57–60.

Boettcher, A.L. (1984) The system SiO_2-H_2O-CO_2: melting, solubility mechanisms of carbon, and liquid structure to high pressures. American Mineralogist, 69, 823–833.

Boettcher, A.L., and Wyllie, P.J. (1968) Jadeite stability measured in the presence of silicate liquids in the system $NaAlSiO_4$-SiO_2-H_2O. Geochimcia et Cosmochimica Acta, 32, 999–1012.

——— (1969) Phase relationships in the system $NaAlSiO_4$-SiO_2-H_2O to 35 kilobars pressure. American Journal of Science, 267, 875–909.

Boettcher, A.L., Windom, K.E., Bohlen, S.R., and Luth, R.W. (1981) Low friction, anhydrous, low- to high-temperature furnace sample assembly for piston-cylinder apparatus. Reviews of Scientific Instruments, 52, 1903–1904.

Boettcher, A.L., Burnham, C. Wayne, Windom, K.E., and Bohlen, S.R. (1982) Liquids, glasses, and the melting of silicates to high pressures. Journal of Geology, 90, 127–138.

Bohlen, S.R., and Boettcher, A.L. (1982) The quartz = coesite transformation: A precise determination and the effects of other components. Journal of Geophysical Research, 87, 7073–7078.

Bohlen, S.R., Boettcher, A.L., and Wall, V.J. (1982) The system albite-H_2O-CO_2: A model for melting and activities of water at high pressures. American Mineralogist, 67, 451–462.

Bohlen, S.R., Boettcher, A.L., Wall, V.J., and Clemens, J.D. (1983) Stability of phlogopite-quartz and sanidine-quartz: A model for melting in the lower crust. Contributions to Mineralogy and Petrology, 83, 270–277.

Brey, G., and Green, D.H. (1977) Systematic study of liquidus phase relations in olivine melilitite + H_2O + CO_2 at high pressures and petrogenesis of an olivine melilitite magma. Contributions to Mineralogy and Petrology, 61, 141–162.

Burnham, C. Wayne. (1979) The importance of volatile constituents. In H.S. Yoder, Jr., Ed., The evolution of the igneous rocks, 439–482. Princeton University Press, New Jersey.

Burnham, C. Wayne, Holloway, J.R., and Davis, N.F. (1969) Thermodynamic properties of water to 1000°C and 10,000 bars. Geological Society of America Special Paper 132.

Cohen, L.H., and Klement, W., Jr., (1967) High-low quartz inversion: Determination to 35 kilobars. Journal of Geophysical Research, 72, 4245–4251.

Chou, I-M. (1978) Calibration of oxygen buffers at elevated *P* and *T* using the hydrogen fugacity sensor. American Mineralogist, 63, 690–703.

de Santis, R., Breedveld, G.J.F., and Prausnitz, J.M. (1974) Thermodynamic properties of aqueous gas mixtures at advanced pressures. Industrial Engineering Chemistry, Process Design and Development, 13, 374–377.

Ebisuzaki, Y., Kass, W.J., and O'Keefe, M. (1968) Solubility and diffusion of hydrogen and deuterium in platinium. Journal of Chemical Physics, 49, 3329–3332.

Eggler, D.H. (1975) CO_2 as a volatile component of the mantle: the system Mg_2SiO_4-SiO_2-H_2O-CO_2. Physics and Chemistry of the Earth, 9, 869–881.

——— (1978) The effect of CO_2 upon partial melting of peridotite in the system Na_2O-CaO-Al_2O_3-MgO-SiO_2-CO_2 to 35 kb with an analysis of melting in a peridotite-H_2O-CO_2 system. American Journal of Science, 278, 305–343.

Eggler, D.H., and Burnham, C. Wayne. (1984) Solution of H_2O in diopside melts: A thermodynamic model. Contributions to Mineralogy and Petrology, 85, 58–66.

Eggler, D.H., and Kadik, A.A. (1979) The system $NaAlSi_3O_8$-H_2O-CO_2 to 20 kbar pressure: I. Compositional and thermodynamic relations of liquids and vapors coexisting with albite. American Mineralogist, 64, 1036–1048.

Eggler, D.H., and Rosenhauer, M. (1978) Carbon dioxide in silicate melts: II. Solubilities of CO_2 and H_2O in $CaMgSi_2O_6$ (diopside) liquids and vapors at pressures to 40 kbar. American Journal of Science, 278, 64–94.

Eggler, D.H., Mysen, B., and Hoering, T.C. (1974) Gas species in sealed capsules in solid media, high-pressure apparatus. Carnegie Institution of Washington Year Book 73, 228–232.

Faile, S.P., and Roy, D.M. (1970) Mechanism of color center destruction in hydrogen impregnated radiation resistant glasses. Materials Research Bulletin, 5, 385–390.

——— (1971) Dissolution of hydrogen in fused silica. American Ceramic Society Journal, 54, 533–534.

Faile, S.P., Schmidt, J.J., and Roy, D.M. (1967) Irradiation effects in glasses: Suppression by synthesis under high-pressure hydrogen. Science, 156, 1593–1595.

Gerlach, T.M. (1982) Interpretation of volcanic gas data from tholeiitic and alkaline mafic lavas. Bulletin Volcanologique, 45, 235–244.

Gerlach, T.M., and Nordlie, B.E. (1975) The C-O-H-S gaseous system, Part I: Composition limits and trends in basaltic cases. American Journal of Science, 275, 353–376.

Goldsmith, J.R., and Jenkins, D.M. (1984) The high-low albite relations revealed by hydrothermal melting and reversal of degree of order. (abs.) EOS (American Geophysical Union Transactions), 65, 307.

Greenwood, H.J. (1975) Buffering of pore fluids by metamorphic reactions. American Journal of Science, 275, 573–593.

Haggerty, S.E., and Toft, P.B. (1985) Native iron in the continental lower crust: Petrological and geophysical implications. Science, 229, 647–649.

Hill, R.E.T., and Boettcher, A.L. (1970) Water in the Earth's mantle: melting curves of basalt-water and basalt–water–carbon dioxide. Science, 167, 980–982.

Holloway, J.R. (1977) Fugacity and activity of molecular species in supercritical fluids. In D.G. Fraser, Ed., Thermodynamics in geology, 161–182. Reidel, Dordrecht, Holland.

Huebner, J.S. (1971) Buffering techniques for hydrostatic systems at elevated pressures. In G.C. Ulmer, Ed., Research techniques for high pressure and high temperature, 123–177. Springer-Verlag, New York.

Kennedy, G.C. (1948) Equilibrium between volatiles and iron oxides in rocks. American Journal of Science, 246, 529–549.

Kennedy, G.C., Wasserburg, G.J., Heard, H.C., and Newton, R.C. (1962) The upper three-phase region in the system SiO_2-H_2O. American Journal of Science, 260, 501–521.

Kerrick, D.M., and Jacobs, G.K. (1981) A modified Redlich-Kwong equation of state for H_2O, CO_2, and H_2O-CO_2 mixtures at elevated pressures and temperatures. American Journal of Science, 281, 735–767.

Luth, W.C., Jahns, R.H., and Tuttle, O.F. (1964) The granite system at pressures of 4 to 10 kilobars. Journal of Geophysical Research, 69, 759–773.

Morse, S.A. (1970) Alkali feldspars with water at 5 kb. Journal of Petrology, 11, 221-251.

Mysen, B.O., and Boettcher, A.L. (1975) Melting of a hydrous mantle: I. Phase relations of natural peridotite at high pressures and temperatures with controlled activities of water, carbon dioxide, and hydrogen. Journal of Petrology, 16, 520–548.

Mysen, B.O., and Virgo, D. (1980) Solubility mechanisms of carbon dioxide in silicate melts: A Raman spectroscopic study. American Mineralogist, 65, 885–899.

Nakamura, Y. (1974) The system SiO_2-H_2O-H_2 at 15 kbar. Carnegie Institution of Washington Year Book 73, 259–263.

Presnall, D.C. (1969) Pressure-volume-temperature measurements on hydrogen from 200°C to 600°C and up to 1800 atmospheres. Journal of Geophysical Research, 74, 6026–6033.

Robie, R.A., Hemingway, B.S., and Fisher, J.D. (1979) Thermodynamic properties of minerals and related substances at 298.15 K (25°C) and one bar (10 pascals) pressure and at higher temperatures (revised 1979). U.S. Geological Survey Bulletin 1452.

Sack, R.O., Carmichael, I.S.E., Rivers, M., and Ghiorso, M.S. (1980) Ferric-ferrous equilibria in natural silicate liquids at 1 bar. Contributions to Mineralogy and Petrology, 75, 369–377.

Shaw, H.R. (1963) Hydrogen–water vapor mixtures: Control of hydrothermal atmospheres by hydrogen osmosis. Science, 139, 1220–1222.

Shaw, H.R., and Wones, D.R. (1964) Fugacity coefficients for hydrogen gas between 0° and 1000°C, for pressures to 300 atm. American Journal of Science, 262, 918–929.

Shettel, D.C. (1973) Solubility of quartz in H_2O-CO_2 fluids at 5 kb and 500°–900°C (abs.) EOS American Geophysical Union Transactions, 54, 480.

Stewart, D.B. (1967) Four-phase curve in the system $CaAl_2Si_2O_8$-

SiO_2-H_2O between 1 and 10 kilobars. Schweizerische Mineralogische und Petrographische Mitteilungen, 47, 35–59.

Stolper, E. (1982) The speciation of water in silicate melts. Geochimica et Cosmochimica Acta, 46, 2609–2620.

Tuttle, O.F., and Bowen, N.L. (1958) Origin of granite in the light of experimental studies in the system $NaAlSi_3O_8$-$KAlSi_3O_8$-SiO_2-H_2O. Geological Society of America Memoir 74.

Welhan, J.A., and Craig, H. (1979) Methane and hydrogen in East Pacific Rise hydrothermal fluids. Geophysical Research Letters, 6, 829–831.

Wyllie, P.J. (1979) Magmas and volatile components. American Mineralogist, 64, 469–500.

Manuscript received April 8, 1985
Manuscript accepted November 4, 1985